ACS OMEGA

http://pubs.acs.org/journal/acsodf

Article

Enhanced Visible-Light-Induced Photocatalytic Activity in M(III)Salophen-Decorated TiO_2 Nanoparticles for Heterogeneous Degradation of Organic Dyes

Abdolreza Rezaeifard,* Masoumeh Rezaei, Narges Keikha, Maasoumeh Jafarpour,* Pinghua Chen, and Hualin Jiang

Cite This: *ACS Omega* 2023, 8, 3821−3834

Read Online

ACCESS | Metrics & More | Article Recommendations | Supporting Information

ABSTRACT: In this work, the construction of two heterojunction photocatalysts by coordinative anchoring of M(salophen)Cl complexes (M = Fe(III) and Mn(III)) to rutile TiO_2 through a silica−aminopyridine linker (SAPy) promotes the visible-light-assisted photodegradation of organic dyes. The degradation efficiency of both cationic rhodamine B (RhB) and anionic methyl orange (MO) dyes by Fe− and Mn−TiO_2-based catalysts in the presence of H_2O_2 under sunlight and low-wattage visible bulbs (12−18 W) is investigated. Anionic MO is more degradable than cationic RhB, and the Mn catalyst shows more activity than its Fe counterpart. Action spectra demonstrate the maximum apparent quantum efficiency (AQY) at 400−450 nm, confirming the visible-light-driven photocatalytic reaction. The enhanced photocatalytic activity might be attributed to the improved charge transfer in the heterojunction photocatalysts evidenced by photoluminescence (PL) and electrochemical impedance spectroscopy (EIS) analyses. A radical pathway for the photodegradation of dyes is postulated based on scavenging experiments and spectral data. This work provides new opportunities for constructing highly efficient catalysts for wastewater treatment.

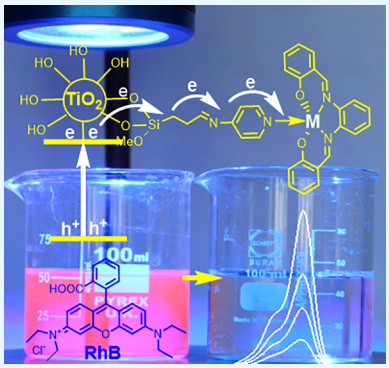

INTRODUCTION

The environmental and health problems of pollution have raised public concerns. Unintentional exposure to various organic and inorganic pollutants may have various harmful effects on the human body and a deleterious effect on the well-being of mankind.[1] Accordingly, in today's scientific world, the removal of pollutants has easily become the center point of research efforts. Given the massive discharge of chemicals and subsequent pollution from various sources such as metallurgy, textile, paper, tannery, and paint industries, the conventional treatment is mostly ineffective and not environmentally compatible.[2] In recent years, semiconductor-mediated photocatalysis as a cost-effective, environmentally friendly, and modern technology has grown rapidly for the degradation of effluents.[3,4] Among heterogeneous photocatalysts, titanium dioxide (TiO_2) as a promising semiconductor photocatalyst has been widely used in wastewater treatment because of its unique photoelectric properties, high chemical stability, low cost, and safety for both humans and the environment.[5] It has been widely used in water and air purification, hydrogen production, electrode material, solar cells, cancer therapy, and self-cleaning of antibacterial materials.[6−14] Among TiO_2 polymorphs, anatase-phase TiO_2 and anatase−rutile-mixed TiO_2 are believed to have superior photocatalytic activity.[15] As a photocatalyst, one major disadvantage of TiO_2 is that it can only be activated by irradiation with ultraviolet (UV) light, i.e., only 5% of the solar energy compared to visible light, owing to its relatively wide band gap (3.2 eV for anatase). Thus, any shift in its optical response from UV to the visible spectral range will have a remarkable positive effect on the practical application of the material. Another problem comes from the transformation from the metastable anatase phase to the thermodynamically stable rutile phase. Thus, it seems that the high stability and smaller band gap (3.05 eV) of the rutile phase extending the absorbance threshold for harvesting more visible light than anatase meet the requirement for practical applications.[15] Besides, due to the rather fast recombination of electron−hole pairs, the quantum efficiencies of TiO_2 in energy conversions are rather poor, leading to the poor photoactivity of TiO_2 even in the UV region.[16] To improve the photocatalytic ability and widen application fields, different preparation methods and a lot of modification methods have been tried, which have been reviewed in several articles.[15−17] Modification of TiO_2 with a Schiff base,[18,19] ascorbic acid (vitamin C),[20−23] g-C_3N_4,[24,25] dendrimer,[26,27] and boron[28] is one of the efforts of our research groups in this area. To extend

Received: September 15, 2022
Accepted: December 29, 2022
Published: January 17, 2023

Scheme 1. Preparation of M(salophen)Cl@SAPy/TiO_2 (M = Fe, Mn) Heterojunction Nanocomposites for Photocatalytic Degradation of Dyes

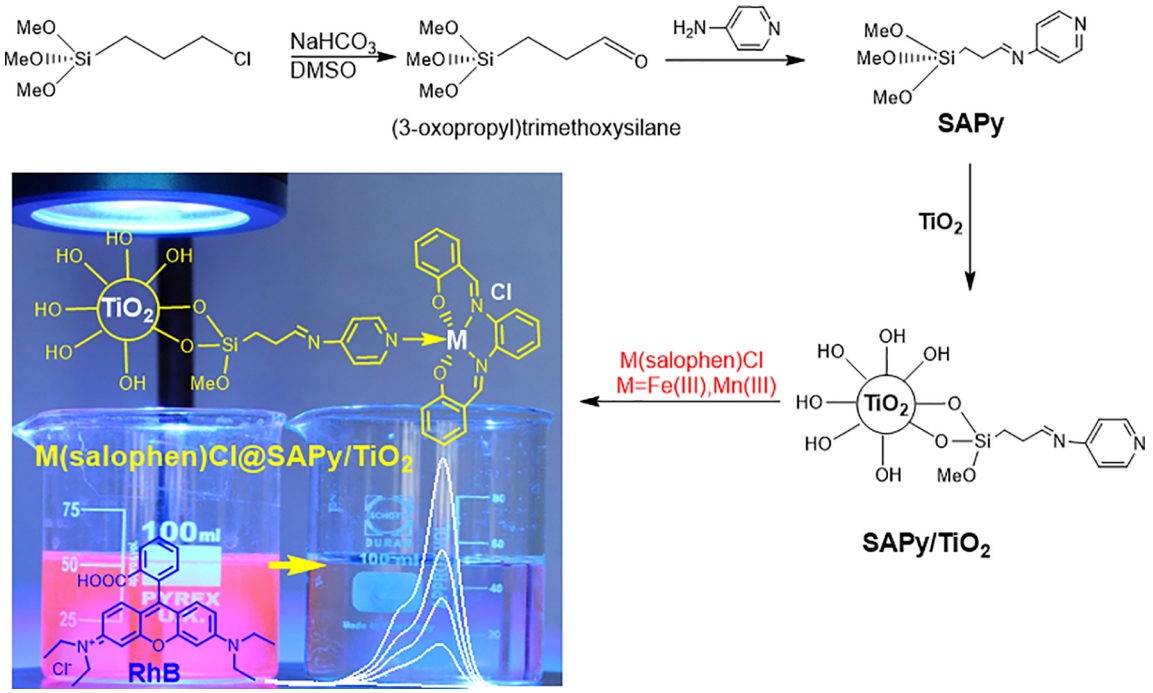

our modification methods and inspired by heme-containing enzymes, recently, we designed a new organosilicon linker (SAPy) by condensation of (3-oxopropyl)trimethoxysilane with 4-aminopyridine (Scheme 1) capable of coordinating to metal complexes of easily made salen- or salophen-type ligands with widespread applications in catalysis.[29] SAPy-functionalized maghemite nanoparticles (γ-Fe_2O_3) were successfully used for the coordinative anchoring of M−salophen complexes (M = Fe, Mn) (M(III)(salophen)Cl@SAPy/Fe_2O_3).[29] However, these magnetic nanocatalysts showed a moderate activity toward oxidative degradation of organic dyes in an aqueous solution of H_2O_2.[29] When we replaced γ-Fe_2O_3 with TiO_2 (Scheme 1, M(salophen)Cl@SAPy/TiO_2), promising results were obtained for visible- and sunlight-assisted degradation of organic dyes, inducing us to present this work. Both cationic and anionic organic dyes are degraded in an aqueous solution of H_2O_2 in the presence of both Fe(III) and Mn(III)salophen-modified TiO_2 nanocomposites. Sunlight and low-wattage visible light bulbs are quite effective in inducing the as-prepared photocatalysts in the dye's degradation process at desired times. Different factors affecting the photocatalytic performance are investigated, and the photoefficiency of the system is assessed by action spectra. The reusability and stability of the photocatalyst are also examined, and a possible photochemical mechanism for the degradation process is proposed.

EXPERIMENTAL SECTION

The procedures for the preparation of (3-oxopropyl)-trimethoxysilane (Scheme 1), SAPy (Scheme 1), TiO_2, and Fe(III)- and Mn(III)(salophen)Cl are given in the Supporting Information.

Fabrication of SAPy/TiO_2. In total, 1.0 g of TiO_2 nanoparticles (Supporting Information) were mixed with 10 mL of ethanol to produce a homogeneously mixed solution. Then, 1.0 g of the SAPy ligand (Supporting Information)[29] in 10 mL of ethanol was added dropwise to the TiO_2 suspension followed by sonication of the mixture for 2 h at 60 °C. The mixture was refluxed for a further 12 h. Finally, the composition was isolated by centrifugation and washed with ethanol, and the resulting precipitate was kept under vacuum at 60 °C for 8 h.

Fabrication of Fe(III)(salophen)Cl@SAPy/TiO_2. To 1.0 g of the SAPy/TiO_2 nanohybrid in 10 mL of ethanol was gradually added 0.5 g of Fe(salophen)Cl (M = Fe, Mn) (a period of 10 min) under ultrasonic agitation at 60 °C followed by refluxing for a further 12 h. Afterward, the product was centrifuged and washed with ethanol followed by drying for 8 h at 60 °C (Scheme 1).

Procedure for Photocatalytic RhB Degradation. In a general procedure, 50 mL of aqueous solution with pH = 3 containing the required concentration of RhB, 5 mg of M(III)(salophen)Cl@SAPy/TiO_2 (M = Fe, Mn), and 62 μL of H_2O_2 solution (30%) was stirred under visible light. The pH was adjusted by the addition of appropriate amounts of NaOH or HCl solution. At given intervals, an appropriate amount of the suspension was taken out and filtered to remove the solid particles before analysis. The concentration of RhB was measured using a spectrophotometer set at a wavelength of maximum absorbance (λ_{max}) of 554 nm. The decoloration ratio (DC%) of RhB was calculated using eq 1.

$$DC = (C_0 - C_t)/C_0 \times 100 \quad (1)$$

where C_0 (mg/L) and C_t (mg/L) are the initial and final RhB concentrations, respectively. The same procedure was conducted for methyl orange at a wavelength of maximum absorbance (λ_{max}) of 517 nm.

Procedure for Determining the Photoefficiency. A full-spectrum 40 W CFL bulb was used as an irradiation source. The filters used in this work are a blue filter (LEYBOLD-HERAEUS GMBH 46811) with lux = 1000 to irradiate with $\lambda \sim 450$ nm; a green filter (LEYBOLD-

https://doi.org/10.1021/acsomega.2c05971
ACS Omega 2023, 8, 3821−3834

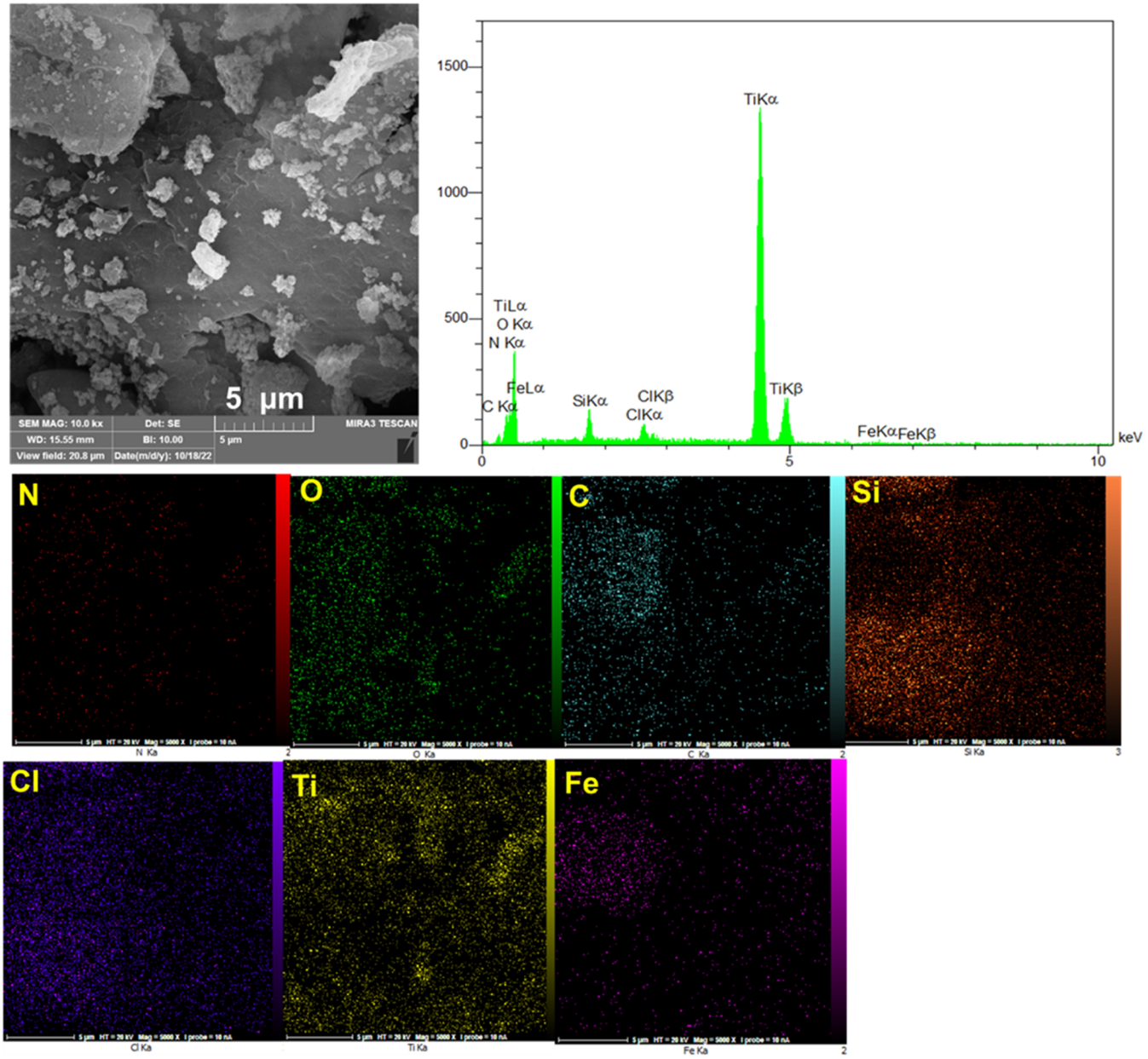

Figure 1. Energy-dispersive X-ray spectrometry (EDS) and elemental mapping at the microstructural level by scanning electron microscopy (SEM) of Fe(salophen)Cl@SAPy/TiO_2.

HERAEUS GMBH 46807) with lux = 1200 to irradiate with $\lambda \sim 530$ nm; a solution mixture of $Cu(OAc)_2$, methyl orange, and $NaNO_2$ with lux = 3720 to irradiate with $\lambda \sim 570$ nm; a solution mixture of Fe(EDTA), $KMnO_4$, and $Cu(OAc)_2$ with lux = 3300 to irradiate with $\lambda \sim 630$ nm; and a solution mixture of methylene blue, phenol red, and $KMnO_4$ with lux = 3200 to irradiate with $\lambda \sim 760$ nm. The degradation of RhB was carried out by the procedure mentioned in the previous section.[30]

RESULTS AND DISCUSSION

Catalyst Characterization. The successful preparation of the Fe(salophen)Cl@SAPy/TiO_2 hybrid was initially confirmed by the detection of its composing elements (C, N, O, Si, Cl, Ti, and Fe) using energy-dispersive X-ray spectrometry (EDS) with elemental mapping at the microstructural level by scanning electron microscopy (SEM, Figure 1). The uniform distribution of the elements can be observed in the hybrid.

Based on the ICP-OES analysis, the precise Fe content of the fabricated hybrid was found to be 1.23% corresponding to 0.22 mmol/g.

X-ray photoelectron spectroscopy (XPS) analysis provided further proof of Fe(salophen)Cl@SAPy/TiO_2 fabrication and useful information about the chemical environment and oxidation state of the elements. The high-resolution XPS spectra of C 1s, O 1s, N 2p, Fe 2p, Cl 2p, Si 2p, and Ti 2p of the as-prepared hybrid are given in Figure 2. The two C 1s signals with binding energies (BEs) of 284.05 (C−C and C═C) and 285.4 (Csp^2−N) were detected.[31] The N 1s spectrum revealed three signals at 397.65, 399.45, and 400.8 eV corresponding to pyridinic and salophen nitrogens as uncoordinated and coordinated to a transition metal.[32−34] The O 1s spectra are deconvoluted into three signals at 529.35,

https://doi.org/10.1021/acsomega.2c05971
ACS Omega 2023, 8, 3821−3834

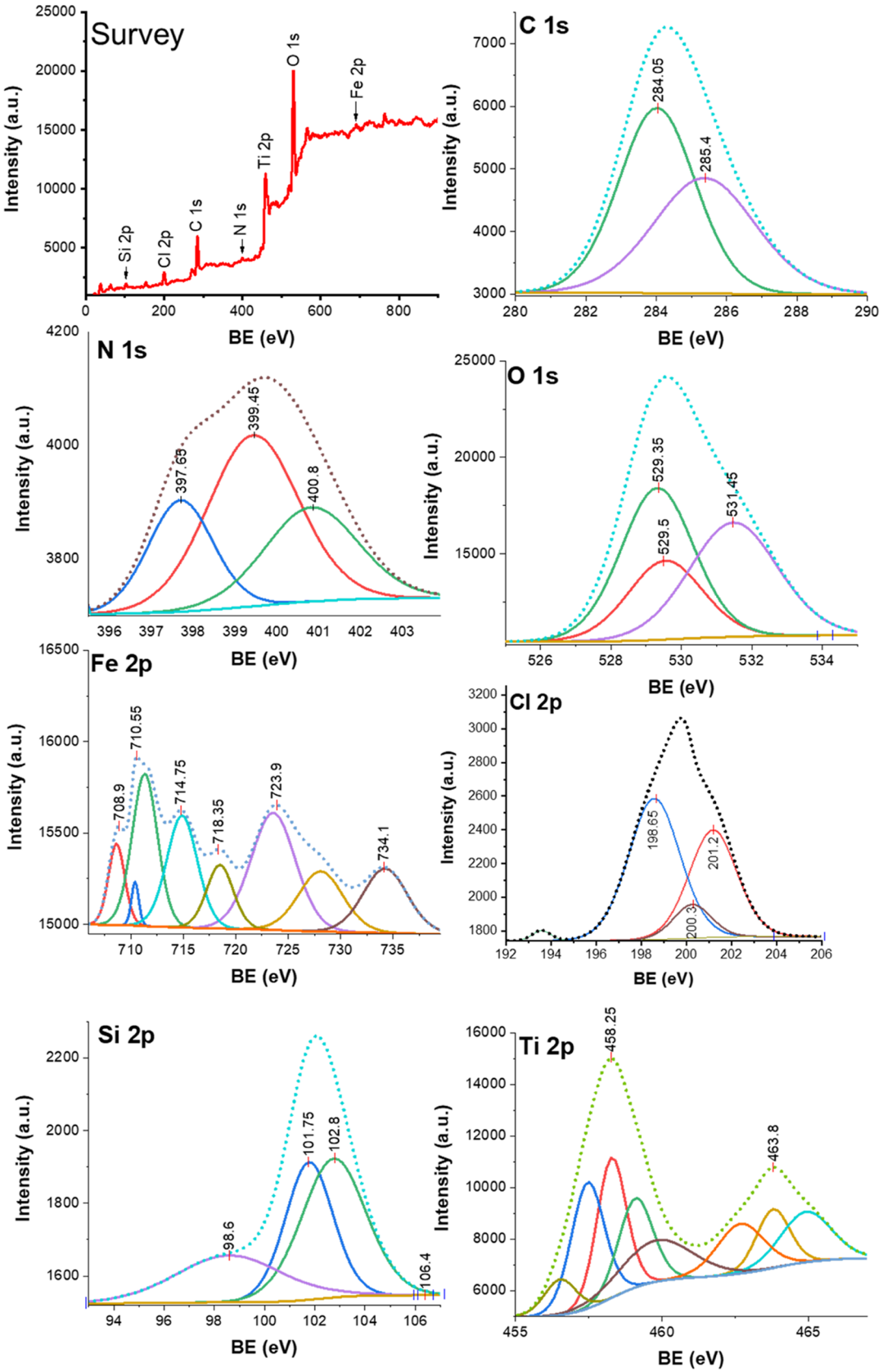

Figure 2. XPS survey and high-resolution spectra of C 1s, N 1s, O 1s, Fe 2p, Cl 2p, Si 2p, and Ti 2p of Fe(salophen)Cl@SAPy/TiO_2.

529.5, and 531.45 eV. The signals at 529 eV are assigned to O atoms bonded in the Ti−O linkage because the Ti−O linkage is a dominant species. The signal with the higher binding energy at 531.45 eV is assigned to the coordinated phenolic oxygen of the salophen ligand or O atoms bonded in the Si−O−Ti linkage.[32,35]

https://doi.org/10.1021/acsomega.2c05971
ACS Omega 2023, 8, 3821−3834

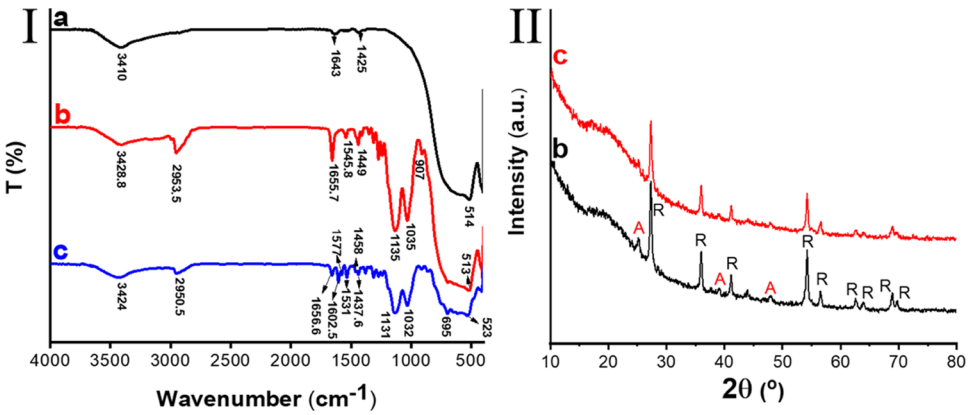

Figure 3. (I) FT-IR spectra of (a) TiO_2, (b) TiO_2/SAPy, and (c) Fe(salophen)Cl@SAPy/TiO_2. (II) XRD pattern of (b) SAPy/TiO_2 and (c) Fe(salophen)Cl@SAPy/TiO_2; "'R"' represents the rutile phase and "'A"' represents the anatase phase.

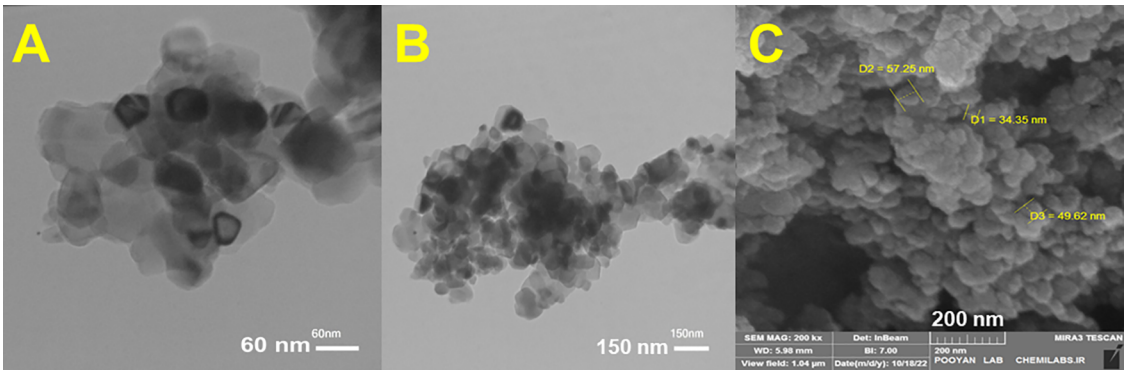

Figure 4. TEM (A, B) and FE-SEM images of the Fe(salophen)Cl@SAPy/TiO_2 nanocomposite.

The Fe 2p spectra contain two main peaks at 710.55 and 723.9 eV corresponding to Fe $2p_{3/2}$ and Fe $2p_{1/2}$ of Fe^{3+}, respectively, along with some contribution of Fe^{2+} (708.9 and 718.35 eV).[36] This was further supported by the Cl 2p spectra. The main signal with the largest area centered at a binding energy of 198.65 eV demonstrates inorganic chlorine (BE < 199 eV)[37] from a chloride salt with Fe^{3+}.[38,39] Si 2p exhibited three signals at binding energies of 98.6, 101.75, and 102.8 eV, indicating the covalent bonding of Si in Si−C, Si−O, and Si−O−Ti, respectively.[40] Main signals of Ti 2p are observed at binding energies of 458.25 eV ($2p_{3/2}$) and 463.8 eV ($2p_{1/2}$) for TiO_2.[24]

The FT-IR spectra and powder X-ray diffraction (PXRD) pattern of Fe(salophen)Cl@SAPy/TiO_2 are depicted in Figure 3 in comparison with precursors. In the FT-IR spectra (Figure 3I), the major bands appeared at 450−775 cm^{-1} in all presented spectra assigned to the stretching vibrations of the Ti−O group, demonstrating the presence of TiO_2 in all three materials (Figure 3Ia−c). The broad peaks at 3410 and 1643 cm^{-1} in Figure 3Ia correspond to the surface-adsorbed water and hydroxyl groups on bare TiO_2, respectively.[20] Figure 3Ib confirms the successful fabrication of the TiO_2/SAPy composite. A peak at 2953 cm^{-1} is attributed to the stretching vibrations of the aliphatic C−H propyl groups of SAPy. The appearance of the peak at 1655.7 cm^{-1} in Figure 3Ib is assigned to the C═N frequency of the imine bond of SAPy.[29] After the attachment of SAPy to the surface of TiO_2, this band shifted to 1656.6 cm^{-1} (Figure 3Ic). The sharp bands at 1035 and 1135 cm^{-1} in SAPy rationalized to the Si−O groups in the linker structure (Figure 3Ib), which shifted slightly to 1032 and 1131 cm^{-1}, respectively, after coordination to the Fe(salophen)Cl complex (Figure 3Ic). Strong evidence for the attachment of the Fe(salophen)Cl complex on the TiO_2 nanoparticles was provided by the emergence of a new band at 1602.5 cm^{-1} (Figure 3Ic), which is characteristic of the imine bonds of the salophen ligand of Fe(salophen)Cl (Figure S1). Other new peaks appeared at 700−800 and 1300−1580 cm^{-1} (Figure 3Ic), which are consistent with those of neat Fe(salophen)Cl (Figure S1).[29]

Figure 3II shows the comparative X-ray diffraction patterns of TiO_2/SAPy (b) and Fe(salophen)Cl@SAPy/TiO_2 (c) in the diffraction angle range of 10−80°. The characteristic diffraction peaks at 27.3° (110), 36° (101), 41° (111), 54.2° (211), 56.7° (220), 62.6° (002), 64° (310), 69 (301), and 69.6° (112) (JCPDS 88-1175) approved the rutile phase (R in Figure 3IIb) of TiO_2 nanoparticles alongside a trace amount of the anatase phase (A in Figure 3IIb) after calcination at 700 °C. Moreover, TiO_2 preserved its crystalline structure during the subsequent surface modification.[41]

Transmission electron microscopy (TEM) and FE-SEM (C) images depicted in Figure 4 revealed cubic particles with sizes ranging between 30 and 60 nm for the Fe(salophen)Cl@SAPy/TiO_2 nanocomposite.

The thermal behavior of the fabricated nanocatalyst was analyzed through thermogravimetric analysis (TGA) from ambient temperature to 800 °C. The TGA curve of Fe(salophen)Cl@SAPy/TiO_2 nanoparticles given in Figure S2 demonstrated its stability up to 250 °C, and the organic parts were removed completely at 600 °C.

https://doi.org/10.1021/acsomega.2c05971
ACS Omega 2023, 8, 3821−3834

Degradation of Dyes. The photocatalytic degradation of RhB as a cationic dye and MO as an anionic dye was conducted in the presence of the Fe(salophen)Cl@SAPy/TiO_2 catalyst and H_2O_2 as a green oxidant under blue LED (12 W) irradiation as a visible light source. UV−vis spectroscopic analysis was performed at different intervals during the photocatalytic degradation to follow the chemical evolution of the solution. The first step for the degradation of pollutants in a heterogeneous photocatalytic process is their adsorption to the surface of the solid catalyst. We left the samples in the dark for ∼60 min and measured the absorbance every 15 min until it was nearly constant. Then, we transferred them into light and measured the absorbance. In the solution with pH = 3 as the optimized pH in this work (vide infra), adsorption of cationic RhB by Fe(salophen)Cl@SAPy/TiO_2 was almost negligible (5%), while 52% of anionic MO was adsorbed on the as-prepared nanocomposite in the dark after 60 min. Accordingly, to avoid errors resulting from the removal adsorption of MO in different control experiments, the reaction conditions were optimized using RhB solution. To exclude the possibility that dye degradation was caused by light radiation and/or H_2O_2, we performed blank experiments where only RhB solution in the absence of the catalyst was radiated with visible light in the absence and presence of H_2O_2. In the absence of a photocatalyst and H_2O_2, the RhB concentration remained almost unaltered after 4 h and decreased slightly in the presence of H_2O_2 under catalyst-free conditions (Table 1 entry 1). The Fe(III)salen complex has been well described as an effective photocatalyst for the degradation of cationic dyes such as RhB under high-power 500 W visible light;[42] nevertheless, the use of the salophen counterpart, Fe(III)salophen, in this work that uses a low-intensity 12 W blue LED did not improve the efficiency (entry 2, 29% after 4 h). Although discrepancies in ligand structures (salen vs salophen) and significant differences in power, intensity, and wavelength range of used bulbs are responsible for such contradistinction in activity, the nature of the true catalyst is a very important issue that has not been well addressed.[42] The oxidative degradation of ligands, difficulties in separating the products, and contamination by residual catalysts are major problems often encountered in the oxidation reactions catalyzed by metal−organic complexes. The fixation of the metal−organic complexes onto different supports to obtain heterogeneous catalysts helps to minimize the problems of industrial disposal and waste treatment. For practical applications of heterogeneous systems, the lifetime of a catalyst and its recovery and reusability are very important factors.[43−48] The attachment of Fe(III)salophen to TiO_2 via SAPy in this work produced a heterogeneous catalyst, (Fe(salophen)Cl@SAPy/TiO_2), which promoted the RhB photodegradation activity of TiO_2 from 62% (entry 3) to 100% (entry 6) and reduced the reaction time from 4 to 2.25 h, i.e., almost double the yield in half the time. Meanwhile, as will be discussed later, the Fe(III)salophen seems to preserve its structural integrity during the reaction. The nonoxidative degradation activity of Fe(salophen)Cl@SAPy/TiO_2 was inferior (entry 5), demonstrating the direct involvement and key role of H_2O_2 in the reaction mechanism (vide infra), a sign for a photo-Fenton system.[49] In the photo-Fenton process, the photodegradation of dyes by Fe^{3+} and H_2O_2 under visible light involves the excitation of the dye followed by the reduction of Fe^{3+} to Fe^{2+}, where the excited dye helps the reduction. Then, the classical Fenton reaction occurs to produce hydroxyl radicals. These radicals are the key species, which facilitate the degradation of the dyes.[50,51] For a neat iron(III) complex, the photo-Fenton process involves two basic steps. The first step is the photoreduction of iron(III) to iron(II) by photoinduced metal−heteroatom bond cleavage[52] or by ligand-to-metal charge transfer.[53] However, for the iron(III) complex attached to TiO_2 like the present system, the photoreduction of iron(III) to iron(II) by photoinduced TiO_2 is a more likely process.[54,55] The reaction of H_2O_2 with iron(II) to produce reactive hydroxyl radicals is the second step.[50,51] Thus, one can conclude that the synergistic effect between Fe(salophen)Cl and TiO_2 promotes the visible light photoactivity of the as-prepared heterojunction nanocomposite (Fe(salophen)Cl@SAPy/TiO_2) in the presence of H_2O_2.

Table 1. Comparing the Catalytic Activity of Fe(salophen)Cl@SAPy/TiO_2 with Parent Materials[a]

entry	catalyst	oxidant	DC%	time (h)
1	catalyst-free	H_2O_2	23	4
2	Fe(salophen)Cl	H_2O_2	29	4
3	TiO_2	H_2O_2	62	4
4	TiO_2/SAPy	H_2O_2	71	4
5	Fe(salophen)Cl@SAPy/TiO_2	-	5	4
6	Fe(salophen)Cl@SAPy/TiO_2	H_2O_2	100	2.25

[a]Fifty milliliters of an aqueous solution of 2 ppm RhB with pH 3.0 containing 62 μL of H_2O_2 and 5 mg of the catalyst was run under a 12 W blue LED.

Several parameters (pH, H_2O_2 concentration, time of reaction, amount of the catalyst) were optimized to perform the photocatalytic degradation of RhB (Figure 5). It is well known that the photocatalytic degradation of an organic pollutant solution is affected significantly by pH, which is caused by the charges and the adsorption behavior of pollutant molecules on the surface of catalysts.[56] The effect of pH on the photodegradation efficiency of RhB was examined in the range of 2−9 under a blue LED in the presence of Fe(salophen)Cl@SAPy/TiO_2/H_2O_2. As shown in Figure 5A, the photodegradation was more efficient in acidic solutions than in alkaline media. The best performance was obtained at pH 3 (92%/2 h), and after that, the removal efficiency decreased significantly and reached 38% at pH 9. The faster formation of Fe(II) in acidic media may be a good reason for such an exhibition[29] because the classic Fenton reaction occurs in the presence of Fe(II) to produce hydroxyl radicals from H_2O_2. However, the stability of the Fe(III)salophen complex in acidic pH[42] is an important issue that should be taken into account.

The effect of the catalyst amount on the photodegradation efficiency was screened, and the results are depicted in Figure 5B. As expected, the photodegradation performance increased with an increase in Fe(salophen)Cl@SAPy/TiO_2 concentration up to 5 mg. Nevertheless, a further increase in the catalyst loading did not improve noticeably the reaction performance caused by a decrease in the accessible active sites on the catalyst surface resulting from the agglomeration of the catalyst nanoparticles. However, limited light penetration resulting from the increased scattering effect may be effective.[56,57] As mentioned earlier, the presence of H_2O_2 is indispensable to triggering the reaction, and the rate and efficiency of photocatalytic degradation are affected by the concentration of H_2O_2.[56,58] Accordingly, some experiments with different concentrations of H_2O_2 were carried out using

https://doi.org/10.1021/acsomega.2c05971
ACS Omega 2023, 8, 3821−3834

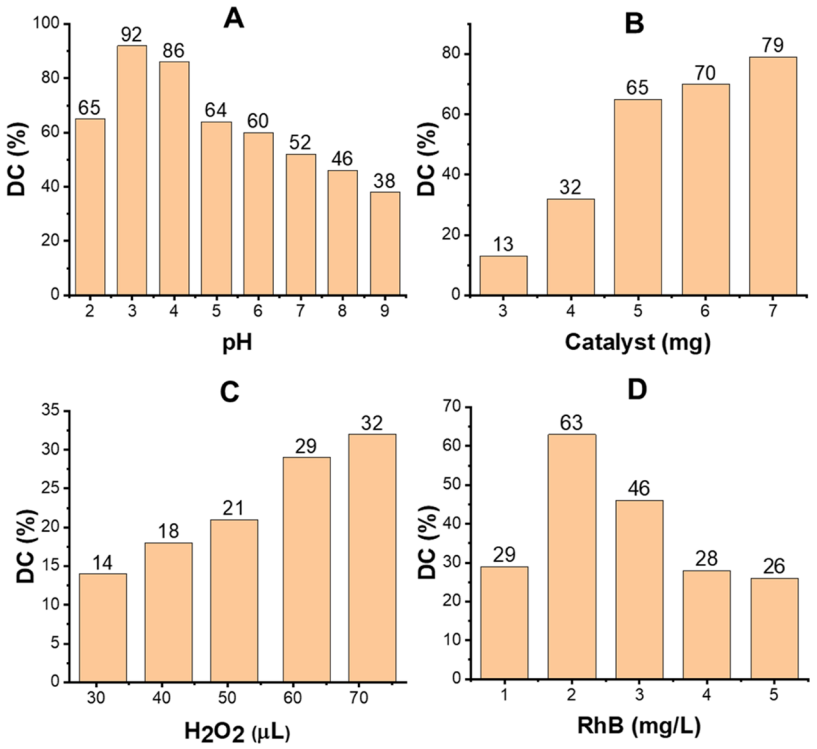

Figure 5. Effect of the initial pH (A), catalyst amount (B), oxidant amount (C), and dye concentration (D) on the degradation rate of RhB at an irradiation time of 1 h except for (A), which was run for 2 h (ultrasonic time: 5 min), pH = 3 except for (A), 5 mg of the catalyst except for (B), H_2O_2: 62 μL except for (C), and 2 mg L^{-1} RhB except for (D).

Table 2. Effect of the Dye Structure and the Metal Center of the Salophen Complex on the Photocatalytic Activity[a]

		Time (min) for 100% DC	
dye	light source[b]	Fe(salophen)Cl@SAPy/TiO_2	Mn(salophen)Cl@SAPy/TiO_2
RhB	Reptile lamp	180	60
	sunlight	30	30
	Actinic BL	60	30
	blue LED	135	50
MO	Reptile lamp	10	25
	sunlight	3	5
	Actinic BL	60	10
	blue LED	135	30

[a]Fifty milliliters of an aqueous solution of 2 ppm RhB with pH 3.0 containing 62 μL of H_2O_2 and 5 mg of the catalyst was run under different light sources. [b]Reptile lamp, LT NARVA (18 W, full range visible light + 4% UV), Actinic BL TL-D Philips (15 W, λ = 366−400 nm), and blue LED, AC86, Z.F.R (12 W, λ_{max} = 505 nm).

Fe(III)(salophen)@SAPy/TiO_2 under blue LED light, and the results are given in Figure 5C. To reach the effective RhB photodegradation at the desired time, the system required 12 mM H_2O_2 (62 μL/50 mL), and the use of a less amount of the oxidant prolonged the reaction. As will be demonstrated in the next sections, H_2O_2 increases the formation rate of hydroxyl radicals in two ways: (1) the reduction of H_2O_2 at the conduction band and (2) self-decomposition by illumination. At low concentrations, H_2O_2 enhances the degradation of compounds due to more efficient generation of hydroxyl radicals and inhibition of electron−hole pair recombination. However, when the concentration of H_2O_2 increases, the electron acceptor reacts with hydroxyl radicals and acts as a scavenger of the photoproduced holes. In addition, in the presence of a high concentration of peroxide, OH radicals preferentially react with the excess of H_2O_2. This undesirable reaction competes with the destruction of the dye chromophore; meanwhile, the radical−radical reaction must also be taken into account.[59]

Finally, the potential of the title photocatalytic system for removing different RhB concentrations was evaluated. Based on the results presented in Figure 5D, to reach the best catalytic performance using Fe(salophen)Cl@SAPy/TiO_2 under optimized conditions (50 mL of an aqueous solution of RhB with a pH of 3.0 containing 62 μL of H_2O_2 and 5 mg of the catalyst under a 12 W blue LED), the RhB concentration should be 2 mg/L. At a lower concentration of the dye, H_2O_2 competes with the dye molecules for the reaction with active species such as OH radicals. On the other hand, at higher dye concentrations, dye molecules are adsorbed on the surface of the catalyst, and a significant amount of irradiation light is absorbed by the dye molecules rather than the photocatalyst particles. The generation of hydroxyl radicals decreases, since the active sites are occupied by dye molecules. The adsorbed

https://doi.org/10.1021/acsomega.2c05971
ACS Omega 2023, 8, 3821−3834

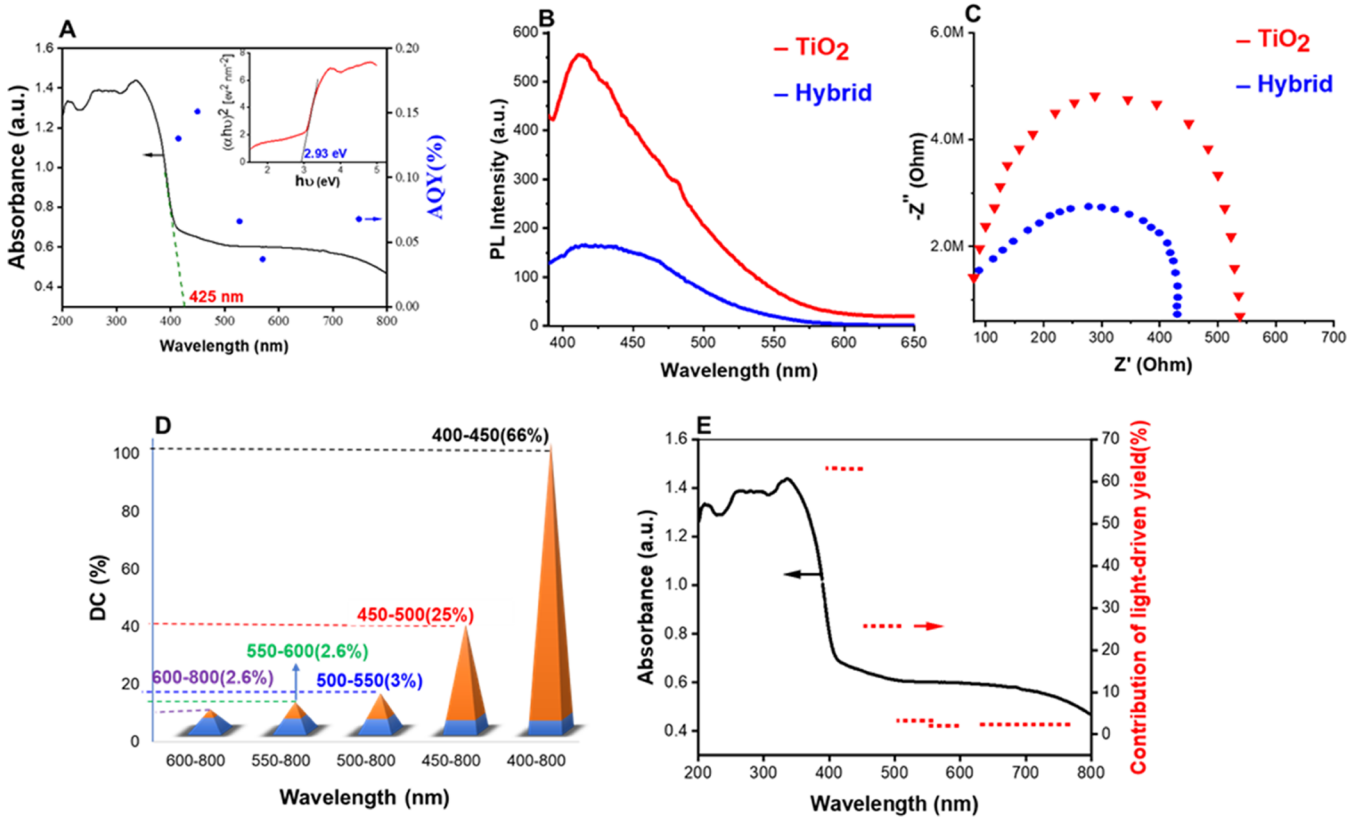

Figure 6. (A) DRS spectra (black curve) and the Tauc plot (inset) of Fe(III)(salophen)Cl@SAPy/TiO_2, and its action spectra (blue dots) for RhB degradation under CFL light. (B) PL spectra of TiO_2 and Fe(III)(salophen)Cl@SAPy/TiO_2 excited at 355 nm; (C) electrochemical impedance spectroscopy using a three-electrode assembly in 2.5 mM $K_4[FeCN_6]\cdot 3H_2O$, 2.5 mM $K_3[FeCN_6]$, and 0.5 M Na_2SO_4 solution;[64] (D) dependence of the photodegradation of RhB on the irradiation wavelength catalyzed by Fe(salophen)Cl@SAPy/TiO_2; and (E) the action spectra of the photocatalytic reaction in which the light-driven conversion is plotted against the irradiation wavelength. The reactions were exposed to CFL light equipped with cutoff filters for 120 min under optimized conditions.

dye on the photocatalyst also inhibits the reaction of adsorbed molecules with the photoinduced positive holes or hydroxyl radicals, since there is no direct contact of the semiconductor with them.[60] Moreover, as the initial concentration of the dye increases, the requirement of an active site needed for the degradation also increases. Since illumination time and amount of the catalyst are constant, the OH radical (primary oxidant) formed on the surface of the photocatalyst is also constant. So, the relative number of free radicals attacking the dye molecules decreases with an increasing amount of the dye.[61] It is notable that the title photocatalytic system proved to be amenable to scalability so that a relatively high RhB concentration of 50 ppm was removed thoroughly using a 25-fold scale procedure at the same time.

Effect of the Dye Structure and the Metal Center of Salophen Complexes. The optimized conditions were employed to assess the photocatalytic activity of Fe(salophen)-Cl@SAPy/TiO_2 in the degradation of RhB and anionic azo dye MO under different visible light sources, and the results are summarized in Table 2. All visible light sources were quite effective in the RhB degradation, and sunlight was the best (100% DC at 30 min), featuring true visible- and sunlight-driven photocatalysis. The photocatalytic degradation of the MO anionic dye was obviously superior to that of RhB, knowing that no color fading occurred in the MO aqueous solution after UV and visible light irradiation under catalyst-free conditions.[62] MO faded rapidly within 10 and 3 min irradiation of the Reptile lamp and sunlight, respectively, whereas fading of RhB took 180 and 30 min, respectively, under the same conditions. The superior photocatalytic degradation of MO to that of RhB may be mainly caused by the high adsorptivity of anionic MO (52% in darkness) by Fe(salophen)Cl@SAPy/TiO_2 based on the results obtained in the darkness. Moreover, it is known that MO degradation is more efficient in an acidic medium (pH ∼3) due to the better sensibility of the protonated form of the dye for the oxidation process.[63]

More interesting results were obtained when Fe(III) was replaced by Mn(III) in the salophen complex. The resulting nanocomposite Mn(III)(salophen)Cl@SAPy/TiO_2 (see the Supporting Information for characterization, Figures S3−S7) effectively degraded both dyes faster than its Fe(III) counterpart; meanwhile, the adsorption amounts of RhB and MO were 5 and 15%, respectively, in darkness. For example, RhB degradation took 60, 30, and 50 min under the Reptile lamp, Actinic BL, and blue LED, respectively, which are significantly less than those in the presence of the Fe(III) counterpart (180, 60, and 135 min, respectively). Almost the same activity was observed for the degradation of MO, which was thoroughly and effectively removed under the photocatalytic influence of Mn(III)(salophen)Cl@SAPy/TiO_2 in less than 10 and 30 min under the Actinic BL and blue LED, respectively. These findings extended the capability scope of this photocatalytic system for the degradation of different types of dyes using different metal centers. Comparing the results with those obtained by the relevant magnetically recoverable

https://doi.org/10.1021/acsomega.2c05971
ACS Omega 2023, 8, 3821−3834

catalysts (M(III)(salophen)Cl@SAPy/γ-Fe_2O_3) in our previous report[29] is worthwhile and confirmed the superiority of the present photocatalytic system. RhB was degraded in moderate yields of 56 and 46.5% in the presence of Mn(III)- and Fe(III)(salophen)Cl@SAPy/γ-Fe_2O_3, respectively, after 70 min,[29] and was removed thoroughly within 30 min under sunlight in the presence of both Fe(III)- and Mn(III)-(salophen)Cl@SAPy/TiO_2. Moreover, we found that Mn-(III)(salophen)Cl@SAPy/γ-Fe_2O_3 is inferior in MO degradation even at a higher temperature of 50 °C (unpublished results), while Mn(III)(salophen)Cl@SAPy/TiO_2 prepared in this work degraded it quite in less than 30 min at room temperature under low power visible light sources. These results affirmed well the superiority of the TiO_2-based M(III)salophen catalyst presented in this work over its magnetic counterpart reported in our previous work.[29] Thus, the effective synergistic effect between TiO_2 and M(salophen)Cl facilitates the charge transfer in the heterojunction photocatalysts, promoting the photocatalytic activity under visible and sunlight irradiation, as will be discussed in the next section.

Photochemical Investigations. The diffuse reflectance UV−vis spectra of Fe(salophen)Cl@SAPy/TiO_2 (DRS, Figure 6, black curve) were recorded to assess the visible light absorption ability and band gap value. It may show the effect of TiO_2 surface modification on the photophysical properties of the fabricated nanocomposite. The absorbance edge of the as-prepared Fe(salophen)Cl@SAPy/TiO_2 shifted to 425 nm corresponding to a band gap value of 2.92 eV (E (eV) = 1239.8/425 nm), which was consistent with the value obtained by the intercept of the tangents to the Tauc plot (2.93 eV). However, the band gap value of the as-prepared hybrid is too close to that of bare rutile TiO_2 (3.05 eV),[15] to justify its superior photocatalytic activity. The effective carrier's separation in the heterojunction M(salophen)Cl@SAPy/TiO_2 hybrid is an important factor in improving photoactivity and can be easily evaluated by photoluminescence (PL) spectroscopy. Quenching of the PL intensity (excited at 355 nm) by 71% obviously showed the efficient electron−hole separation resulting from the charge transfer between the TiO_2 core and M(salophen)Cl through the SAPy linker, which is expected to increase the photochemical activity of the fabricated hybrid (Figure 6B).[24] This was further supported by electrochemical impedance spectroscopy (EIS) measurements (Figure 6C).[64] Typically, a semicircle with a larger radius refers to a higher charge transfer resistance of the electrode. Therefore, the EIS result depicted in Figure 6C concluded that the charge transfer resistance (R_{ct}) of the Fe(salophen)Cl@SAPy/TiO_2 electrode is smaller than that of TiO_2, confirming the higher conductivity and charge transfer in the as-prepared hybrid than those in bare TiO_2.[65]

The wavelength-dependent photocatalytic performance of Fe(salophen)Cl@SAPy was screened in the degradation of RhB exposed to a full-spectrum CFL lamp equipped with cutoff filters (Figure 6A blue dots). The apparent quantum efficiency (AQY) that expresses the photoefficiency of the system is defined as AQY = N/I_0 (N, decomposed RhB molecules, molecules per s; I_0, the volumetric flux of photons, photons per second).[63] It was screened for the RhB decomposition at different wavelengths in the visible light region (400−800 nm) considering the contribution of the thermal effect. The photoefficiency of RhB decomposition showed a maximum value at about 400−450 nm and then decreased (Figure 6A blue dots), which is consistent with the diffuse reflectance absorption spectrum (Figure 6A black curve). These results demonstrated that the RhB decomposition performance was wavelength-dependent and suggested that the photocatalyst was efficient in the visible light region under the conditions used in this study.[66,67]

We also investigated the relative contribution of thermal and photochemical processes in the RhB degradation reaction (Figure 6D). The photochemical reactions were performed under a 40 W CFL lamp equipped with cutoff filters. Light contributed to the conversion efficiency was determined by subtracting the conversion in the dark from the total conversion under the light. Without any filter, the degradation reaction of RhB can reach 100% within 120 min (Figure S8). When the wavelength ranges were limited to 450−800, 500−800, 550−800, and 600−800 nm, the efficiency decreased to 37, 13, 10, and 7.5%, respectively. The contribution of 400−450 nm light accounts for about 66% ((95 − 32)/95 × 100) of the total light-induced yield. Also, light in wavelength ranges of 450−500, 500−550, 550−600, and 600−800 nm accounts for 25, 3, 2.6, and 2.6% of the light-induced yield, respectively (Figure 6D).[68] These values are well consistent with the DRS of the title nanocomposite (Figure 6E). Light in the wavelength range of 400−450 nm provides the most photoinduced conversion for RhB degradation, which is in excellent agreement with DRS and action spectra presented in Figure 6A and E. It can be attributed to the strong absorption of Fe(III)(salophen)Cl@SAPy/TiO_2 below 400 nm (337 nm), which was further confirmed by exposing the reaction to ACTINIC BL light (λ = 366−400 nm). RhB faded within 60 min, which is half the time needed for CFL and one-third the time needed for Reptile light; both of them possess almost full visible light spectra, confirming once again that the best performance of RhB degradation is around 400 nm.

Process Features and Mechanistic Aspects. To elucidate the active species and reaction mechanism, some control experiments were performed in the presence of common scavengers. As shown in Figure 7A, DC% reduced significantly to 39, 33, and 28% in the presence of t-Butyl alcohol (TBA), ammonium oxalate (AO), and ascorbic acid (AA) as efficient scavengers of hydroxyl radicals ($^{\bullet}OH$), holes (h^+), and superoxide radicals ($O_2^{\bullet-}$), respectively, indicating the effective involvement of $^{\bullet}OH$, h^+, and $O_2^{\bullet-}$ in the reaction mechanism.[69] Knowing that the electron paramagnetic Resonance (epr) is not applicable to capture the radical species in this reaction media,[42] the involvement of OH radicals in the reaction mechanism was established by the reaction of terephthalic acid (nonfluorescent) with OH radicals, yielding fluorescent 2-hydroxyl terephthalic acid (HTA).[70] As shown in Figure 7B, upon excitation of a reaction mixture containing H_2O_2 and the catalyst at 315 nm, the PL intensity grew gradually at 455 nm resulting from the formation of 2-hydroxy terephthalic acid, testifying the generation of OH radicals during the reaction. By removing H_2O_2 from the reaction mixture under the same conditions, the PL intensity at 455 nm decreased significantly (Figure 7C), which was due to a decrease in the OH radical concentration. This result demonstrated that OH radicals are generated mainly from H_2O_2, testifying to the classic Fenton reaction.[50,51]

Based on these results and the relevant mechanism reported previously,[50−55] a radical mechanism can be proposed as eqs 2−5. The use of Fe(III)salophen can improve the separation of

https://doi.org/10.1021/acsomega.2c05971
ACS Omega 2023, 8, 3821−3834

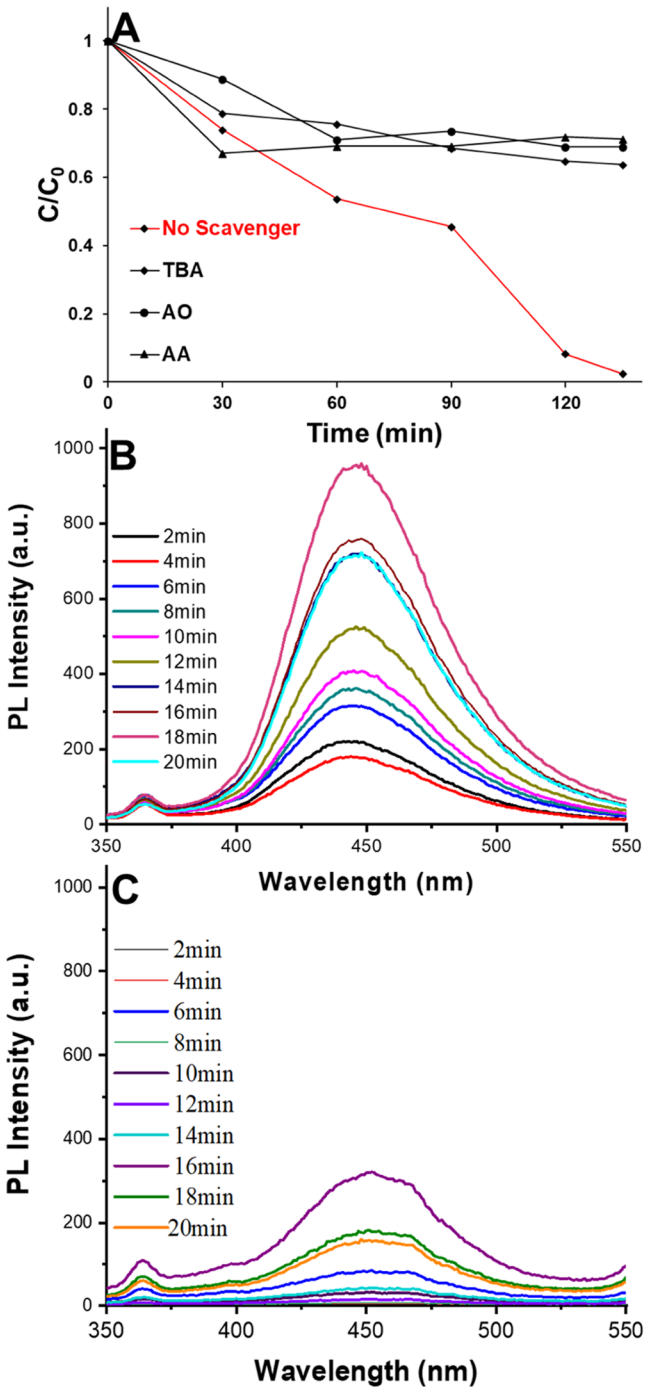

Figure 7. (A) Effect of different radical scavengers on RhB degradation in the presence of Fe(salophen)Cl@SAPy/TiO_2 and H_2O_2 under blue LED light irradiation (TBA: *t*-butyl alcohol, AO: ammonium oxalate, and AA: ascorbic acid). (B, C) The photoluminescence spectra of 2-hydroxy-terephthalic acid formed by the reaction of terephthalic acid (TPA) with in situ-generated $^{\bullet}OH$ radicals at different irradiation times in the presence (B) and in the absence (C) of H_2O_2.

photoproduced e^-–h^+. The Fe(III) species, of course, coordinated with the salophen ligand plays a very important role in the electron transfer process. As outlined in eqs 2 and 3, the photoinduced oxidation of H_2O_2 by iron(III)salophen yields $HO_2^{\bullet}$, whereas the reduced metal salophen (Fe(II)-salophen) is oxidized by H_2O_2 and $O_2^{\bullet-}$ via a dark process to generate $^{\bullet}OH$, both of which are active species for dye degradation (eq 5).[54,71] It was not possible to detect the photoreduced Fe^{3+} species during the reaction caused by its rapid reoxidation by H_2O_2. Thus, the involvement of iron centers in the reaction mechanism was assessed by the Fe 2p XPS spectra of the used catalyst after the reaction (Figure S9). The signal at 708.9 eV in the fresh catalyst (Figure S9) corresponds to some sharing of Fe^{2+} shifted partially to 709.1 eV in the used catalyst; nevertheless, a significant reduction in the intensity of Fe^{2+} signals compared to Fe^{3+} signals (711.3 eV) was observed. Further, the Fe^{3+} signals of the fresh catalyst centered at 711.3 ($2p_{3/2}$) and 723.68 eV ($2p_{1/2}$) shifted partially to the higher binding energies of 711.52 and 725.15 eV, respectively, after the reaction (Figure S9). Thus, the oxidation role of Fe centers seems inevitable.

On the other hand, the dye molecule can rapidly capture the valence band holes or, alternatively, react with surface OH radicals (eqs 4 and 5).[55] The more effective interaction of anionic dye MO with the positive species of $Ti{-}OH^{+\cdot}$ may be further evidence for its higher degradation efficiency. However, the more negative HOMO and LUMO of MO than those of RhB,[72] facilitating the reduction of Fe(III) to Fe(II) through charge transfer from the excited dye (MO) to Fe(salophen)Cl attached to TiO_2 nanoparticles, should be taken into account for the rapid degradation of MO under visible light irradiation. Thus, the excited M(salophen)Cl and dye molecules act as electron relay mediators to improve the overall electron transfer efficiency in the heterojunction photocatalyst, leading to the significant promotion in the visible-light-driven degradation efficiency.

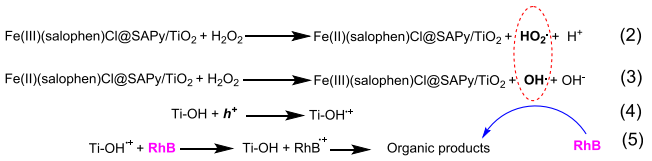

The chromophore structure of activated $RhB^{+\cdot}$ is efficiently destroyed by the abovementioned radical species produced using the visible-light-assisted Fe(salophen)Cl@SAPy/TiO_2/H_2O_2 system, as detected by the GC–MS analysis of the filtrate (Figure S10). The lack of any peak with a molecular mass of 433 and the emergence of many peaks with low intensities pertinent to the smaller organic molecules confirmed the efficient destruction of RhB.[42,73] The predominant peak that appeared at a retention time of 15.6 min corresponds to an intermediate with a molecular mass of 281 (Figure S10), demonstrating the cleavage of the RhB chromophore.[74] As evidenced by m/z values of 259, 241, 207, 147, 129, 112, 83, and 57, the prolonged reaction degrades the aromatic intermediates into small organic molecules via ring opening.[73−75] Thus, M(salophen)Cl@SAPy/TiO_2 is efficient enough to degrade successfully the chromophore of the dye in the presence of H_2O_2 under low-wattage visible bulbs.

Stability and Reusability of the Catalyst. The reusability and stability of the photocatalyst are two key factors for industrial applications.[43−48] Initially, the heterogeneous nature of the catalyst was confirmed by a filtration experiment (Figure S11A). For this purpose, the reaction mixture was exposed to a blue LED for 30 min while stirring, and after that, it was filtered off. DC% was 25% at this time. Then, the filtrate was allowed to stir under the blue LED for a further 105 min, and DC% reached ultimately 36%, almost equal to that under catalyst-free conditions (Table 1, entry 1).

https://doi.org/10.1021/acsomega.2c05971
ACS Omega 2023, 8, 3821−3834

ICP-OES analysis provided more evidence for the heterogeneity of the catalytic system as well as the stability of the catalyst during the reaction. The Fe content of the used catalyst was found to be 1.19%, featuring the negligible leaching of Fe(III)salophen (3.25%) during the reaction. These promising results induced us to evaluate the recyclability of the catalytic system. At each step after the completion of the reaction, the catalyst was washed with distilled water, dried under vacuum, and used directly without further purification. The catalyst proved to preserve its activity during at least four runs. DC% reached 98, 95, and 91% after the second, third, and fourth runs, respectively, within 135 min under blue LED light (Figure S11B). More important is the structural stability of Fe(salophen)Cl@SAPy/TiO_2 during the photocatalytic reactions, which was confirmed by a comparison of the EDX and FT-IR spectra of the used and fresh catalyst (Figure S11C,D). However, some changes in the Fe signals in the XPS spectra of Fe 2p (Figure S9) and a significant reduction in the intensity of Fe^{2+} signals raise some questions regarding the possible changes in the coordination environment of Fe centers that should be further investigated.

Thus, the high degradation activity of the M(III)(salophen)-Cl@SAPy/TiO_2 heterojunction photocatalyst toward both cationic and anionic dyes using visible and sunlight irradiation as safe energy sources and H_2O_2 as a green oxidant along with desired recyclability and scalability qualifies all requirements of an efficient photocatalytic system for environmental cleanup and makes it a promising candidate for industrial applications. These benefits are further highlighted when the results and reaction conditions presented in this work are compared with the previously relevant published works. Some of them use high-wattage UV and visible light (150−300 W), some employ concentrated H_2O_2 (50−400 mM), and most of them are just applicable for the degradation of RhB as a cationic dye (Table S1).

CONCLUSIONS

In summary, M(salophen)Cl (M = Fe(III) and Mn(III)) anchored coordinatively on rutile TiO_2 via the SAPy linker (M(III)(salophen)Cl@SAPy/TiO_2) promoted efficiently the photocatalytic activity to degrade efficiently organic dyes under visible light. TEM and SEM images proved the nanostructured morphology of the as-prepared catalyst (30−60 nm). The degradation of cationic RhB and anionic MO dyes under sunlight and low-wattage visible light irradiation was carried out in the presence of both Fe(III)- and Mn(III)-based catalysts. Low-wattage visible light sources were effective in inducing the photocatalyst for degradation of dyes, and sunlight showed the best performance featuring visible- and sunlight-driven photocatalysis. Adsorption of MO on the title catalysts was more (15−52%) than that of RhB (5%) with the Fe(III)-based catalyst (52%) higher than that of the Mn(III) counterpart (15%). The photocatalytic degradation performance of MO was superior to that of RhB under the same conditions, and the Mn(III)-based catalyst showed more activity than its Fe(III) counterpart toward both cationic and anionic dyes. The wavelength-dependent photocatalytic efficiency of the title photocatalyst was in excellent agreement with UV−vis spectra (DRS) and the light in the wavelength of 400−450 nm provided the most photoinduced conversion for RhB degradation. The photoluminescence (PL) and electrochemical impedance spectroscopy (EIS) analyses revealed the improved charge transfer between the TiO_2 core and the M(III)salophen complex through the SAPy linker, which caused the effective carrier's separation in the hybrid heterojunction, promoting its photocatalytic activity. Pathways for the photocatalytic degradation of dyes by M(III)-(salophen)Cl@SAPy/TiO_2 and Ti−OH were proposed according to active species determined by scavenging experiments and spectral data. The catalytic system was amenable to scalability and recyclability, and the photocatalyst preserved its activity and stability during the reaction. Thus, this catalytic system is expected to be applied in the practical treatment of wastewater on a large scale in the future.

ASSOCIATED CONTENT

Supporting Information

The Supporting Information is available free of charge at https://pubs.acs.org/doi/10.1021/acsomega.2c05971.

Instrumentation; experimental synthetic procedures; additional analyses of Fe(III) and Mn(III)(salophen)-Cl@SAPy/TiO_2 used in this work; UV−vis spectral change; scavenging experiments; GC trace; MS spectra; comparative table; and PL spectra (PDF)

AUTHOR INFORMATION

Corresponding Authors

Abdolreza Rezaeifard − *Catalysis Research Laboratory, Department of Chemistry, Faculty of Science, University of Birjand, Birjand 97179-414, Iran;* orcid.org/0000-0002-8717-9036; Email: rrezaeifard@birjand.ac.ir, rrezaeifard@gmail.com

Maasoumeh Jafarpour − *Catalysis Research Laboratory, Department of Chemistry, Faculty of Science, University of Birjand, Birjand 97179-414, Iran;* orcid.org/0000-0002-9946-5013; Email: mjafarpour@birjand.ac.ir

Authors

Masoumeh Rezaei − *Catalysis Research Laboratory, Department of Chemistry, Faculty of Science, University of Birjand, Birjand 97179-414, Iran*

Narges Keikha − *Catalysis Research Laboratory, Department of Chemistry, Faculty of Science, University of Birjand, Birjand 97179-414, Iran*

Pinghua Chen − *Key Laboratory of Jiangxi Province for Persistent Pollutants Control and Resources Recycle, Nanchang 330063, P. R. China; Department of Environmental and Chemical Engineering, Nanchang Hangkong University, Nanchang 330063, P. R. China;* orcid.org/0000-0003-2738-1723

Hualin Jiang − *Key Laboratory of Jiangxi Province for Persistent Pollutants Control and Resources Recycle, Nanchang 330063, P. R. China; Department of Environmental and Chemical Engineering, Nanchang Hangkong University, Nanchang 330063, P. R. China;* orcid.org/0000-0001-5711-1252

Complete contact information is available at: https://pubs.acs.org/10.1021/acsomega.2c05971

Notes

The authors declare no competing financial interest.

https://doi.org/10.1021/acsomega.2c05971
ACS Omega 2023, 8, 3821−3834

■ ACKNOWLEDGMENTS

Support of this work by the Research Council of the University of Birjand and the "Iran National Science Foundation" (Grant No. 96005005) is highly appreciated.

■ REFERENCES

(1) Xu, H.; Jia, Y.; Sun, Z.; Su, J.; Liu, Q. S.; Zhou, Q.; Jiang, G. Environmental Pollution, A Hidden Culprit for Health Issues. *Eco-Environ. Health* **2022**, *1*, 31−45.
(2) Ahmed, M.; Mavukkandy, M. O.; Giwa, A.; Elektorowicz, M.; Katsou, E.; Khelifi, O.; Naddeo, V.; Hasan, S. W. Recent Developments in Hazardous Pollutants Removal from Wastewater and Water Reuse within a Circular Economy. *npj Clean Water* **2022**, *5*, 12.
(3) Jiang, H.; Wang, Q.; Chen, P.; Zheng, H.; Shi, J.; Shu, H.; Liu, Y. Photocatalytic Degradation of Tetracycline by Using a Regenerable (Bi) BiOBr/rGO Composite. *J. Cleaner Prod.* **2022**, *339*, No. 130771.
(4) Liu, X.; Zhu, L.; Wang, X.; Meng, X. Photocatalytic Degradation of Wastewater by Molecularly Imprinted Ag_2S-TiO_2 with High-Selectively. *Sci. Rep.* **2020**, *10*, No. 1192.
(5) Fujishima, A.; Rao, T. N.; Tryk, D. A. Titanium Dioxide Photocatalysis. *J. Photochem. Photobiol. C* **2000**, *1*, 1−21.
(6) Ghodsi, F. E.; Tepehan, F. Z.; Tepehan, G. G. Study of Time Effect on the Optical Properties of Spin-Coated CeO_2-TiO_2 Thin Films. *Sol. Energy Mater. Sol. Cells* **2001**, *68*, 355−364.
(7) Luan, Y.; Jing, L.; Meng, Q.; Nan, H.; Luan, P.; Xie, M.; Feng, Y. Synthesis of Efficient Nanosized Rutile TiO_2 and Its Main Factors Determining Its Photodegradation Activity: Roles of Residual Chloride and Adsorbed Oxygen. *J. Phys. Chem. C* **2012**, *116*, 17094−17100.
(8) Wang, R.; Shen, J.; Zhang, W.; Liu, Q.; Zhang, M.; Tang, H.; et al. Build-in Electric Field Induced Step-Scheme TiO_2/$W_{18}O_{49}$ Heterojunction for Enhanced Photocatalytic Activity under Visible-Light Irradiation. *Ceram. Int.* **2020**, *46*, 23−30.
(9) Gracia, F.; Holgado, J. P.; Contreras, L.; Girardeau, T.; González-Elipe, A. R. Optical and Crystallisation Behaviour of TiO_2 and V/TiO_2 Thin Films Prepared by Plasma and Ion Beam Assisted Methods. *Thin Solid Films* **2003**, *429*, 84−90.
(10) Kaplan, R.; Erjavec, B.; Pintar, A. Enhanced Photocatalytic Activity of Single-Phase, Nanocomposite and Physically Mixed TiO_2 Polymorphs. *Appl. Catal., A* **2015**, *489*, 51−60.
(11) Alkaim, A. F.; Kandiel, T. A.; Hussein, F. H.; Dillert, R.; Bahnemann, D. W. Solvent-Free Hydrothermal Synthesis of Anatase TiO_2 Nanoparticles with Enhanced Photocatalytic Hydrogen Production Activity. *Appl. Catal., A* **2013**, *466*, 32−37.
(12) Malekkiani, M.; Ravari, F.; Heshmati Jannat Magham, A.; Dadmehr, M.; Groiss, H.; Hosseini, H. A.; Sharif, R. Fabrication of Graphene-Based TiO_2@ CeO_2 and CeO_2@ TiO_2 Core- Shell Heterostructures for Enhanced Photocatalytic Activity and Cytotoxicity. *ACS Omega* **2022**, *7*, 30601−30621.
(13) Liu, R.; Wu, L.; Liu, H.; Zhang, Y.; Ma, J.; Jiang, C.; Duan, T. High-Efficiency Photocatalytic Degradation of Tannic Acid Using TiO_2 Heterojunction Catalysts. *ACS Omega* **2021**, *6*, 28538−28547.
(14) Liu, X.; Zhang, H.; Liu, C.; Chen, J.; Li, G.; An, T.; Wong, P.-K.; Zhao, H. UV and Visible Light Photoelectrocatalytic Bactericidal Performance of 100%{1 1 1} Faceted Rutile TiO_2 Photoanode. *Catal. Today* **2014**, *224*, 77−82.
(15) Daghrir, R.; Drogui, P.; Robert, D. Modified TiO_2 for Environmental Photocatalytic Applications: A Review. *Ind. Eng. Chem. Res.* **2013**, *52*, 3581−3599.
(16) Cheng, H.; Xu, W. Recent Advances in Modified TiO_2 for Photo-Induced Organic Synthesis. *Org. Biomol. Chem.* **2019**, *17*, 9977−9989.
(17) Kumar, S. G.; Devi, L. G. Review on Modified TiO_2 Photocatalysis under UV/visible Light: Selected Results and Related Mechanisms on Interfacial Charge Carrier Transfer Dynamics. *J. Phys. Chem. A* **2011**, *115*, 13211−13241.
(18) Jafarpour, M.; Kargar, H.; Rezaeifard, A. A Cobalt Schiff Base Complex on TiO 2 Nanoparticles as an Effective Synergistic Nanocatalyst for Aerobic C-H Oxidation. *RSC Adv.* **2016**, *6*, 25034−25046.
(19) Jafarpour, M.; Kargar, H.; Rezaeifard, A. A Synergistic Effect of a Cobalt Schiff Base Complex and TiO_2 Nanoparticles on Aerobic Olefin Epoxidation. *RSC Adv.* **2016**, *6*, 79085−79089.
(20) Jafarpour, M.; Rezaeifard, A.; Ghahramaninezhad, M.; Feizpour, F. Dioxomolybdenum (VI) Complex Immobilized on Ascorbic Acid Coated TiO_2 Nanoparticles Catalyzed Heterogeneous Oxidation of Olefins and Sulfides. *Green Chem.* **2015**, *17*, 442−452.
(21) Pourmorteza, N.; Jafarpour, M.; Feizpour, F.; Rezaeifard, A. Cu (Ii) Vitamin C Tunes Photocatalytic Activity of TiO_2 Nanoparticles for Visible Light-Driven Aerobic Oxidation of Benzylic Alcohols. *RSC Adv.* **2020**, *10*, 12053−12059.
(22) Feizpour, F.; Jafarpour, M.; Rezaeifard, A. Band Gap Modification of TiO_2 Nanoparticles by Ascorbic Acid-Stabilized Pd Nanoparticles for Photocatalytic Suzuki–Miyaura and Ullmann Coupling Reactions. *Catal. Lett.* **2019**, *149*, 1595−1610.
(23) Pourmorteza, N.; Jafarpour, M.; Feizpour, F.; Rezaeifard, A. Cu (II)-Vitamin C-Complex Catalyzed Photo-Induced Homocoupling Reaction of Aryl Boronic Acid in Base-Free and Visible Light Conditions. *RSC Adv.* **2022**, *12*, 4931−4938.
(24) Jafarpour, M.; Feizpour, F.; Rezaeifard, A.; Pourmorteza, N.; Breit, B. Tandem Photocatalysis Protocol for Hydrogen Generation/Olefin Hydrogenation Using Pd-G-C_3N_4-Imine/TiO_2 Nanoparticles. *Inorg. Chem.* **2021**, *60*, 9484−9495.
(25) Pourmorteza, N.; Jafarpour, M.; Feizpour, F.; Rezaeifard, A. TiO2 Nanoparticles Decorated with Co-Schiff Base-g-C3N4 as an Efficient Photocatalyst for One-Pot Visible Light-Assisted Synthesis of Benzimidazoles. *RSC Adv.* **2022**, *12*, 22526−22541.
(26) Eskandari, A.; Jafarpour, M.; Rezaeifard, A.; Salimi, M. A Dendritic TiO_2-Co (II) Nanocomposite Based on the Melamine Catalyzed One-Pot Aerobic Photocatalytic Synthesis of Benzimidazoles. *New J. Chem.* **2018**, *42*, 6449−6456.
(27) Eskandari, A.; Jafarpour, M.; Rezaeifard, A.; Salimi, M. Supramolecular Photocatalyst of Palladium (II) Encapsulated within Dendrimer on TiO_2 Nanoparticles for Photo-Induced Suzuki-Miyaura and Sonogashira Cross-Coupling Reactions. *Appl. Organomet. Chem.* **2019**, *33*, No. e5093.
(28) Niu, P.; Wu, G.; Chen, P.; Zheng, H.; Cao, Q.; Jiang, H. Optimization of Boron Doped TiO_2 as an Efficient Visible Light-Driven Photocatalyst for Organic Dye Degradation with High Reusability. *Front. Chem.* **2020**, *8*, 172.
(29) Keikha, N.; Rezaeifard, A.; Jafarpour, M. Heterogeneous Fenton-like Activity of Novel Metallosalophen Magnetic Nanocomposites: Significant Anchoring Group Effect. *RSC Adv.* **2019**, *9*, 32966−32976.
(30) Mokhtari, R.; Rezaeifard, A.; Jafarpour, M.; Farrokhi, A. Visible-Light Driven Catalase-like Activity of Blackberry-Shaped $\{Mo_{72}Fe_{30}\}$ Nanovesicles: Combined Kinetic and Mechanistic Studies. *Catal. Sci. Technol.* **2018**, *8*, 4645−4656.
(31) Nikookar, M.; Rezaeifard, A.; Jafarpour, M.; Grzhegorzhevskii, K. V.; Ostroushko, A. A. A Top-down Design for Easy Gram Scale Synthesis of Melem Nano Rectangular Prisms with Improved Surface Area. *RSC Adv.* **2021**, *11*, 38862−38867.
(32) Burness, J. H.; Dillard, J. G.; Taylor, L. T. X-Ray Photoelectron Spectroscopic Study of Cobalt (II) Schiff Base Complexes and Their Oxygenation Products. *J. Am. Chem. Soc.* **1975**, *97*, 6080−6088.
(33) Osadchii, D. Y.; Olivos-Suarez, A. I.; Bavykina, A. V.; Gascon, J. Revisiting Nitrogen Species in Covalent Triazine Frameworks. *Langmuir* **2017**, *33*, 14278−14285.
(34) Artyushkova, K. Misconceptions in Interpretation of Nitrogen Chemistry from X-Ray Photoelectron Spectra. *J. Vac. Sci. Technol. A* **2020**, *38*, 031002.
(35) Hsu, J.-C.; Wang, P. W.; Lee, C.-C. X-Ray Photoelectron Spectroscopy Study of Thin TiO_2 Films Cosputtered with Al. *Appl. Opt.* **2006**, *45*, 4303−4309.

https://doi.org/10.1021/acsomega.2c05971
ACS Omega 2023, 8, 3821−3834

(36) Yamashita, T.; Hayes, P. Analysis of XPS Spectra of Fe^{2+} and Fe^{3+} Ions in Oxide Materials. *Appl. Surf. Sci.* **2008**, *254*, 2441−2449.
(37) Araujo, J. R.; Archanjo, B. S.; de Souza, K. R.; Kwapinski, W.; Falcão, N. P. S.; Novotny, E. H.; Achete, C. A. Selective Extraction of Humic Acids from an Anthropogenic Amazonian Dark Earth and from a Chemically Oxidized Charcoal. *Biol. Fertil. Soils* **2014**, *50*, 1223−1232.
(38) Blomquist, J.; Helgeson, U.; Moberg, L. C.; Folkesson, B.; Larsson, R. ESCA and Mössbauer Spectra of Some Iron (III) Betadiketonates and Tetraphenylporphyrin Iron (III) Chloride. *Inorg. Chim. Acta* **1983**, *69*, 17−23.
(39) Kim, Y. I.; Hatfield, W. E. Electrical, Magnetic and Spectroscopic Properties of Tetrathiafulvalene Charge Transfer Compounds with Iron, Ruthenium, Rhodium and Iridium Halides. *Inorg. Chim. Acta* **1991**, *188*, 15−24.
(40) Kaur, A.; Chahal, P.; Hogan, T. Selective Fabrication of SiC/Si Diodes by Excimer Laser under Ambient Conditions. *IEEE Electron Device Lett.* **2016**, *37*, 142−145.
(41) Hanaor, D. A. H.; Sorrell, C. C. Review of the Anatase to Rutile Phase Transformation. *J. Mater. Sci.* **2011**, *46*, 855−874.
(42) Gazi, S.; Rajakumar, A.; Singh, N. D. P. Photodegradation of Organic Dyes in the Presence of [Fe (III)-Salen] Cl Complex and H_2O_2 under Visible Light Irradiation. *J. Hazard. Mater.* **2010**, *183*, 894−901.
(43) Rezaeifard, A.; Jafarpour, M.; Naeimi, A.; Haddad, R. Aqueous Heterogeneous Oxygenation of Hydrocarbons and Sulfides Catalyzed by Recoverable Magnetite Nanoparticles Coated with Copper (II) Phthalocyanine. *Green Chem.* **2012**, *14*, 3386−3394.
(44) Marakatti, V. S.; Gaigneaux, E. M. Recent Advances in Heterogeneous Catalysis for Ammonia Synthesis. *ChemCatChem* **2020**, *12*, 5838−5857.
(45) Leadbeater, N. E.; Marco, M. Preparation of Polymer-Supported Ligands and Metal Complexes for Use in Catalysis. *Chem. Rev.* **2002**, *102*, 3217−3274.
(46) Cole-Hamilton, D. J. Homogeneous Catalysis–New Approaches to Catalyst Separation, Recovery, and Recycling. *Science* **2003**, *299*, 1702−1706.
(47) Rezaeifard, A.; Jafarpour, M.; Farshid, P.; Naeimi, A. Nanomagnet-Supported Partially Brominated Manganese-Porphyrin as a Promising Catalyst for the Selective Heterogeneous Oxidation of Hydrocarbons and Sulfides in Water. *Eur. J. Inorg. Chem.* **2012**, *2012*, 5515−5524.
(48) Orege, J. I.; Oderinde, O.; Kifle, G. A.; Ibikunle, A. A.; Raheem, S. A.; Ejeromedoghene, O.; Okeke, E. S.; Olukowi, O. M.; Orege, O. B.; Fagbohun, E. O.; et al. Recent Advances in Heterogeneous Catalysis for Green Biodiesel Production by Transesterification. *Energy Convers. Manage.* **2022**, *258*, No. 115406.
(49) Ameta, S.; Ameta, R. *Advanced Oxidation Processes for Wastewater Treatment: Emerging Green Chemical Technology*; Academic Press, 2018.
(50) Xie, Y.; Chen, F.; He, J.; Zhao, J.; Wang, H. Photoassisted Degradation of Dyes in the Presence of Fe^{3+} and H_2O_2 under Visible Irradiation. *J. Photochem. Photobiol. A* **2000**, *136*, 235−240.
(51) Wu, K.; Xie, Y.; Zhao, J.; Hidaka, H. Photo-Fenton Degradation of a Dye under Visible Light Irradiation. *J. Mol. Catal., A* **1999**, *144*, 77−84.
(52) Lang, K.; Lu\vnák, S. Photocatalytic Degradation of 4-Chlorophenoxyacetic Acid in the Presence of an Iron Complex and Hydrogen Peroxide. *Photochem. Photobiol. Sci.* **2002**, *1*, 588−591.
(53) Kunkely, H.; Vogler, A. Photoredox Reactivity of Iron (III) Phenolates in Aqueous Solution Induced by Ligand-to-Metal Charge Transfer Excitation. *Inorg. Chem. Commun.* **2003**, *6*, 1335−1337.
(54) Huang, H.; Gu, X.; Zhou, J.; Ji, K.; Liu, H.; Feng, Y. Photocatalytic Degradation of Rhodamine B on TiO_2 Nanoparticles Modified with Porphyrin and Iron-Porphyrin. *Catal. Commun.* **2009**, *11*, 58−61.
(55) Molinari, A.; Amadelli, R.; Antolini, L.; Maldotti, A.; Battioni, P.; Mansuy, D. Phororedox and Photocatalytic Processes on Fe (III)-Porphyrin Surface Modified Nanocrystalline TiO_2. *J. Mol. Catal. A* **2000**, *158*, 521−531.
(56) Reza, K. M.; Kurny, A. S. W.; Gulshan, F. Parameters Affecting the Photocatalytic Degradation of Dyes Using TiO_2: A Review. *Appl. Water Sci.* **2017**, *7*, 1569−1578.
(57) Hoffmann, M. R.; Martin, S. T.; Choi, W.; Bahnemann, D. W. Environmental Applications of Semiconductor Photocatalysis. *Chem. Rev.* **1995**, *95*, 69−96.
(58) Bauer, R.; Waldner, G.; Fallmann, H.; Hager, S.; Klare, M.; Krutzler, T.; Malato, S.; Maletzky, P. The Photo-Fenton Reaction and the TiO_2/UV Process for Waste Water Treatment- Novel Developments. *Catal. Today* **1999**, *53*, 131−144.
(59) Konstantinou, I. K.; Albanis, T. A. TiO_2-Assisted Photocatalytic Degradation of Azo Dyes in Aqueous Solution: Kinetic and Mechanistic Investigations: A Review. *Appl. Catal., B* **2004**, *49*, 1−14.
(60) Daneshvar, N.; Salari, D.; Khataee, A. R. Photocatalytic Degradation of Azo Dye Acid Red 14 in Water: Investigation of the Effect of Operational Parameters. *J. Photochem. Photobiol. A* **2003**, *157*, 111−116.
(61) Mengyue, Z.; Shifu, C.; Yaowu, T. Photocatalytic Degradation of Organophosphorus Pesticides Using Thin Films of TiO_2. *J. Chem. Technol. Biotechnol.* **1995**, *64*, 339−344.
(62) Ishigaki, T.; Nakada, Y.; Tarutani, N.; Uchikoshi, T.; Tsujimoto, Y.; Isobe, M.; Ogata, H.; Zhang, C.; Hao, D. Enhanced Visible-Light Photocatalytic Activity of Anatase-Rutile Mixed-Phase Nano-Size Powder given by High-Temperature Heat Treatment. *R. Soc. Open Sci.* **2020**, *7*, No. 191539.
(63) Kudo, A.; Miseki, Y. Heterogeneous Photocatalyst Materials for Water Splitting. *Chem. Soc. Rev.* **2009**, *38*, 253−278.
(64) Chen, P.; Wang, M.; Li, G.; Jiang, H.; Rezaeifard, A.; Jafarpour, M.; Wu, G.; Rao, B. Construction of ZIF-67-On-UiO-66 Catalysts as a Platform for Efficient Overall Water Splitting. *Inorg. Chem.* **2022**, *61*, 18424−18433.
(65) Wang, S.; Zhang, J.; Gharbi, O.; Vivier, V.; Gao, M.; Orazem, M. E. Electrochemical Impedance Spectroscopy. *Nat. Rev. Methods Primers* **2021**, *1*, 41.
(66) Nikookar, M.; Rezaeifard, A.; Grzhegorzhevskii, K. V.; Jafarpour, M.; Khani, R. Melem Nanorectangular Prism-Modified $\{Mo_{72}Fe_{30}\}$ Nanocapsule as a Visible-Light-Assisted Photocatalyst for Catalase-Like Activity. *ACS Appl. Nano Mater.* **2022**, *5*, 7917−7931.
(67) Rezaeifard, A.; Mokhtari, R.; Garazhian, Z.; Jafarpour, M.; Grzhegorzhevskii, K. V. Tetrahedral Keggin Core Tunes the Visible Light-Assisted Catalase-Like Activity of Icosahedral Keplerate Shell. *Inorg. Chem.* **2022**, *61*, 7878−7889.
(68) Feizpour, F.; Jafarpour, M.; Rezaeifard, A. A Tandem Aerobic Photocatalytic Synthesis of Benzimidazoles by Cobalt Ascorbic Acid Complex Coated on TiO_2 Nanoparticles under Visible Light. *Catal. Lett.* **2018**, *148*, 30−40.
(69) Schneider, J. T.; Firak, D. S.; Ribeiro, R. R.; Peralta-Zamora, P. Use of Scavenger Agents in Heterogeneous Photocatalysis: Truths, Half-Truths, and Misinterpretations. *Phys. Chem. Chem. Phys.* **2020**, *22*, 15723−15733.
(70) Bubacz, K.; Kusiak-Nejman, E.; Tryba, B.; Morawski, A. W. Investigation of OH Radicals Formation on the Surface of TiO_2/N Photocatalyst at the Presence of Terephthalic Acid Solution. Estimation of Optimal Conditions. *J. Photochem. Photobiol. A* **2013**, *261*, 7−11.
(71) Ranjit, K. T.; Willner, I.; Bossmann, S.; Braun, A. Iron (III) Phthalocyanine-Modified Titanium Dioxide: A Novel Photocatalyst for the Enhanced Photodegradation of Organic Pollutants. *J. Phys. Chem. B* **1998**, *102*, 9397−9403.
(72) Zulys, A.; Adawiah, A.; Gunlazuardi, J.; Yudhi, M. D. L. Light-Harvesting Metal-Organic Frameworks (MOFs) La-PTC for Photocatalytic Dyes Degradation. *Bull. Chem. React. Eng. Catal.* **2021**, *16*, 170−178.
(73) Garazhian, Z.; Rezaeifard, A.; Jafarpour, M.; Farrokhi, A. $\{Mo_{72}Fe_{30}\}$ Nanoclusters for the Visible-Light-Driven Photocatalytic Degradation of Organic Dyes. *ACS Appl. Nano Mater.* **2020**, *3*, 648−657.

https://doi.org/10.1021/acsomega.2c05971
ACS Omega 2023, 8, 3821−3834

(74) Rajalakshmi, S.; Pitchaimuthu, S.; Kannan, N.; Velusamy, P. Enhanced Photocatalytic Activity of Metal Oxides/β-Cyclodextrin Nanocomposites for Decoloration of Rhodamine B Dye under Solar Light Irradiation. *Appl. Water Sci.* **2017**, *7*, 115−127.
(75) Liu, T.; Wang, L.; Lu, X.; Fan, J.; Cai, X.; Gao, B.; Miao, R.; Wang, J.; Lv, Y. Comparative Study of the Photocatalytic Performance for the Degradation of Different Dyes by $ZnIn_2S_4$: Adsorption, Active Species, and Pathways. *RSC Adv.* **2017**, *7*, 12292−12300.

https://doi.org/10.1021/acsomega.2c05971
ACS Omega 2023, 8, 3821−3834